J|A|C|S ARTICLES

Published on Web 10/09/2009

Dynamic Structural Changes in a Molecular Zeolite-Supported Iridium Catalyst for Ethene Hydrogenation

Alper Uzun and Bruce C. Gates*

Department of Chemical Engineering and Materials Science, University of California, Davis One Shields Avenue, Davis, California 95616

Received August 3, 2009; E-mail: bcgates@ucdavis.edu

Abstract: The structure of a catalyst often changes as a result of changes in the reactive environment during operation. Examples include changes in bulk phases, extended surface structures, and nanoparticle morphologies; now we report real-time characterization of changes in the structure of a working supported catalyst at the molecular level. Time-resolved extended X-ray absorption fine structure (EXAFS) data demonstrate the reversible interconversion of mononuclear iridium complexes and tetrairidium clusters inside zeolite Y cages, with the structure controlled by the C_2H_4/H_2 ratio during ethene hydrogenation at 353 K. The data demonstrate break-up of tetrairidium clusters into mononuclear complexes indicated by a decrease in the Ir−Ir coordination number in ethene-rich feed. When the feed composition was switched to first equimolar and then to a H_2-rich ($C_2H_4/H_2 = 0.3$) feed, the EXAFS spectra show the reformation of tetrairidium clusters as the Ir−Ir coordination number increased again. When the feed composition was cycled from ethene-rich to H_2-rich, the predominant species in the catalyst cycled accordingly. Evidence confirming the structural change is provided by IR spectra of iridium carbonyls formed by probing of the catalyst with CO. The data are the first showing how to tune the structure of a solid catalyst at the molecular scale by choice of the reactant composition.

Introduction

Determination of relationships between structure and performance of solid catalysts is often challenging because (a) multiple structures are present, and identification of those responsible for catalysis may be difficult, and (b) the reactive environment influences the catalyst structure. Examples of (b) occurring at various structural levels include the following: (1) photoemission electron microscopy[1] and ellipsomicroscopy[2] demonstrate how changes in gas-phase reactant composition control microscopic pattern formation during CO oxidation catalysis on Pt(110) (the effects include uniform oscillations, intermittent cascades of amplitude defects, and regular patterns of clusters and standing waves); (2) transmission electron micrographs demonstrate dynamic, reversible changes in the morphology of supported copper nanocrystals in a methanol synthesis catalyst in response to switches in the environment from oxidizing to reducing;[3] and (3) X-ray diffraction patterns, laser Raman spectra, and electron paramagnetic resonance spectra demonstrate the conversion of a metastable bulk phase in a solid oxide catalyst for *n*-butane oxidation to another bulk phase resulting from changes in the feed composition.[4]

Thus, there are examples showing how changes in the reaction environment change extended surface structures, nanoparticle morphologies, and bulk phases of catalysts, but there is a lack of examples showing such changes in solid catalysts at the molecular scale, and our goal was to test for them—a goal that is beyond the reach of microscopy, because images of functioning catalysts at this scale are unattainable, and also beyond the reach of spectroscopy, which characterizes smears of intrinsically nonuniform species in the typical solid catalyst.

Here we overcome the latter limitation, presenting spectroscopic data tracking molecular-scale variations in a supported catalyst synthesized precisely to have essentially uniform catalytic sites;[5] our data show that these can be switched between mononuclear metal complexes and metal clusters. Because uniform catalytic sites require uniform supports, we chose a crystalline porous solid, a zeolite. An unprecedented degree of uniformity among supported catalytic species was demonstrated by dynamic ^{13}C NMR spectra of zeolite-supported rhodium diethene species.[6] We used this same support, highly dealuminated zeolite Y, and prepared anchored iridium species that are isostructural with the anchored rhodium species. The catalyst was synthesized by the reaction of $Ir(C_2H_4)_2(acac)$[7] (acac is $CH_3COCHCOCH_3$) (**1**) with the zeolite, giving an essentially molecular supported metal complex that catalyzes ethene hydrogenation,[5] a reaction that takes place under conditions so mild that these species are resistant to (auto)reduction and

(1) Kim, M.; Bertram, M.; Pollman, M.; von Oertzen, A.; Mikhailov, A. S.; Rotermund, H. H.; Ertl, G. *Science* **2001**, *292*, 1357–1360.
(2) Wolff, J.; Papathanasiou, A. G.; Kevrekidis, I. G.; Rotermund, H. H.; Ertl, G. *Science* **2001**, *294*, 134–137.
(3) Hansen, P. L.; Wagner, J. B.; Helveg, S.; Rostrup-Nielsen, J. R.; Clausen, B. S.; Topsøe, H. *Science* **2002**, *295*, 2053–2055.
(4) Conte, M.; Budroni, G.; Bartley, J. K.; Taylor, S. H.; Carley, A. F.; Schmidt, A.; Murphy, D. M.; Girgsdies, F.; Ressler, T.; Schlögl, R.; Hutchings, G. J. *Science* **2006**, *313*, 1270–1273.
(5) Uzun, A.; Bhirud, V. A.; Kletnieks, P. W.; Haw, J. F.; Gates, B. C. *J. Phys. Chem. C* **2007**, *111*, 15064–15073.
(6) Ehresmann, J. O.; Kletnieks, P. W.; Liang, A.; Bhirud, V. A.; Bagatchenko, O. P.; Lee, E. J.; Klaric, M.; Gates, B. C.; Haw, J. F. *Angew. Chem., Int. Ed.* **2006**, *45*, 574–576.
(7) Bhirud, V. A.; Uzun, A.; Kletnieks, P. W.; Craciun, R.; Haw, J. F.; Dixon, D. A.; Olmstead, M. M.; Gates, B. C. *J. Organomet. Chem.* **2007**, *692*, 2107–2113.

aggregation to form iridium particles.[8a] But these complexes can be converted into clusters well approximated as tetrairidium,[9,10] which also catalyze ethene hydrogenation.[10] An advantage of iridium over rhodium is that the rhodium, in contrast to the iridium, is readily converted into mixtures of clusters of various sizes.[11] We characterized the functioning catalyst in flow reactors by extended X-ray absorption fine structure (EXAFS) and infrared (IR) spectroscopies, showing that the iridium complexes can be transformed into clusters and back into mononuclear complexes, depending on the composition of the reactive atmosphere of ethene and H_2. Others have used EXAFS spectroscopy to follow changes in catalyst structures resulting from changes in reactive atmospheres,[10a,b,11−14] but their data do not identify the changing working catalytic species.

Results and Discussion

Structural Characterization of Initially Prepared Zeolite Y-Supported Iridium Ethene Complex. Data reported earlier[5] characterize the initial zeolite-supported iridium diethene complex prepared by the reaction of **1** with dealuminated zeolite Y. IR spectra indicate the presence of ethene ligands, a result that is confirmed by the presence of an Ir−C contribution with a coordination number of 4 determined by EXAFS spectroscopy; the EXAFS data further indicate the bonding, on average, of each $Ir(C_2H_4)_2$ complex to the zeolite via two Ir−O bonds.[5]

Formation of Iridium Clusters from Mononuclear Iridium Complexes. Time-resolved EXAFS data recorded during the temperature ramp to 353 K with the sample in flowing H_2 demonstrate the formation of Ir−Ir bonds accompanied by the breaking of Ir−C and Ir−O bonds—this cluster formation requires migration of Ir atoms on the zeolite surface (and between the cages).[12] The final Ir−Ir coordination number was 3, indicating the formation of clusters well approximated as Ir_4, on average, and the Ir−Ir bonding distance was 2.65 ± 0.02 Å. IR data indicate the presence of ethylidyne and di-σ-bonded ethene ligands; these require two or more metal sites, confirming the presence of iridium clusters.[12] The X-ray absorption near edge structure (XANES) data recorded simultaneously with the EXAFS data include sharply defined isosbestic points indicating the transformation of one species to another (thus, we infer the conversion of almost uniform mononuclear iridium complexes to another almost uniform species, tetrairidium clusters).[12] Although one would expect the formation of intermediate species such as dimers during this transition, the data do not give any evidence of intermediates.[15] Therefore, we infer that at any time during the transition, we make a good approximation by assuming that the Ir atoms were present either in mononuclear complexes or tetrairidium clusters, and the average information obtained by time-resolved EXAFS data represents the change in the concentrations of these species.

Break-Up of Iridium Clusters into Mononuclear Iridium Complexes. Time-resolved EXAFS data show the break-up of the clusters in flowing C_2H_4 at 353 K; when the flow was switched from H_2 to ethene, the Ir−Ir coordination number decreased from 3 to an undetectably small value as the clusters broke up into mononuclear complexes. The switching between mononuclear iridium complexes and clusters is reversible.[12]

Chemistry of Cluster Formation and Break-Up. The formation of the clusters from the mononuclear iridium complexes in H_2 is clearly a reduction; literature data[10c] demonstrate that when the treatment is carried out at a high temperature (773 K, much higher than that of our experiments, which were carried out at temperatures up to 353 K), the reduction proceeds all the way to iridium metal (in the form of particles). Details of the mechanism of the reduction are not elucidated fully by our results, but the data do show that the ethene ligands on the mononuclear species were hydrogenated during the reduction, to give ethyl ligands and then gas-phase ethane,[12] evidently opening up bonding sites to facilitate Ir−Ir bond formation. As the clusters formed, the Ir−O coordination number decreased, which implies a loosening of the metal−support bonding and the corresponding migration of the iridium that led to the cluster formation. As the iridium was reduced, the hydrogen must have been oxidized, no doubt by the process of spillover, whereby surface OH groups were formed on the zeolite support. IR spectra of the samples (Supporting Information) demonstrate the increase in intensity of the silanol groups, confirming this inference.

Some insight into the cluster break-up emerges from a comparison of the approximate energies of Ir−Ir bonds in the clusters and Ir−(π-bonded C_2H_4) bonds in the resultant complexes. A rough approximation of the Ir−Ir bond dissociation energy, based on data characterizing iridium metal, is reported to be 26.5 kcal/mol,[8b] and the energy of dissociation of one ethene ligand from iridium in $Ir(C_2H_4)_2$(acac) has been calculated by density functional theory to be 47 kcal/mol.[7] Thus, we infer that the strong bonding of ethene to iridium in the complexes provides a driving force for the oxidative fragmentation of the clusters by ethene. The mechanism of this fragmentation reaction is not known, but we might suggest that it involves hydrocarbon ligands and reverse spillover in a process resembling the reverse of the cluster formation. IR spectra of the silanol groups (Supporting Information) confirm the reverse spillover process.

Catalytic Activity of Zeolite-Supported Mononuclear $Ir(C_2H_4)_2$ Complexes for Ethene Hydrogenation. The zeolite-supported mononuclear iridium complexes formed from the reaction of $Ir(C_2H_4)_2$(acac) with the zeolite-catalyzed ethene hydrogenation in a once-through flow reactor in the presence of 40 mbar of ethene and 40 mbar of H_2 (in helium at atmospheric pressure) flowing at a rate of 100 mL/min (the mass of catalyst was 30 mg and the Ir content was 1.0 wt %). These experiments were carried out at a lower temperature (294 K) than that at which the cluster formation and break-up described above were observed. The apparent ethene conversion in the catalytic reaction (determined by an a gas chromatographic analysis of the product stream) was initially approximately 20%, but this value is an overestimate, because it was influenced by the presence of ethene formed by desorption from the catalyst.

(8) (a) Finney, E. E.; Finke, R. G. *Chem. Mater.* **2008**, *20*, 1956–1970. (b) Aiken III, J. D.; Lin, Y.; Finke, R. G. *J. Mol. Catal. A: Chem.* **1996**, *114*, 29–51.
(9) Xu, Z.; Xiao, F.-S.; Purnell, S. K.; Alexeev, O.; Kawi, S.; Deutsch, S. E.; Gates, B. C. *Nature* **1994**, *372*, 346–348.
(10) (a) Argo, A. M.; Odzak, J. F.; Lai, F. S.; Gates, B. C. *Nature* **2002**, *415*, 623–626. (b) Argo, A. M.; Odzak, J. F.; Gates, B. C. *J. Am. Chem. Soc.* **2003**, *125*, 7107–7115. (c) Grundwaldt, J.-D.; Kappen, P.; Basini, L.; Clausen, B. S. *Catal. Lett.* **2002**, *78*, 13–21.
(11) Liang, A. J.; Gates, B. C. *J. Phys. Chem. C* **2008**, *112*, 18039–18049.
(12) Uzun, A.; Gates, B. C. *Angew. Chem., Int. Ed.* **2008**, *47*, 9245–9248.
(13) Bare, S. R.; Ressler, T. *Adv. Catal.* **2009**, *52*, 339–465.
(14) Evans, J.; Luig-Molina, A.; Tromp, M. *MRS Bull.* **2007**, *32*, 1038–1043.
(15) Iridium dimers were detected as intermediate structures as the $Ir(CO)_2$ complexes were transforming into $Ir_4(CO)_{12}$ clusters in highly dehydrated NaY zeolite in the presence of flowing CO (Li, F.; Gates, B. C. *J. Phys. Chem. B* **2004**, *108*, 11259−11264). But evidently the chemistry is not entirely comparable to that reported here, as the zeolite is different, and our data do not provide any evidence of the presence of such intermediate species.

After about 5 h onstream, any influence of desorbed ethene ligands became negligible, and conversion in the flow reactor was approximately 5%. This conversion was almost a steady-state value, but, thereafter, there was a slow, gradual decrease in the conversion, consistent with slow changes in the ligand environment of the iridium. EXAFS data characterizing the catalyst after 10 h of operation gave no evidence of Ir−Ir contributions, indicating that the mononuclear complexes stayed intact during the operation.[5] During the subsequent operation at a near steady state when the conversion was 4%, the turnover frequency was 0.07 (mol C_2H_4) × s^{-1} × (mol Ir)$^{-1}$.

Catalytic Activity of Zeolite-Supported Iridium Clusters. The sample consisting of supported clusters approximated as Ir_4, prepared by treatment of the supported mononuclear iridium complexes in flowing H_2 during a temperature ramp to 353 K (after they were cooled to the catalytic reaction temperature of 294 K in flowing helium), was also tested as a catalyst for ethene hydrogenation. The reaction conditions matched those stated in the preceding paragraph. The data show that the apparent initial ethene conversion was approximately 12%, but this value could reflect ethene in the product stream formed from hydrocarbon ligands initially present on the clusters. After 3 h on stream in the flow reactor, the conversion was 3%, and this was a steady-state value that was maintained in subsequent operation (Supporting Information). The steady-state turnover frequency was calculated by assuming that each Ir_4 cluster was a catalytically active species; the value was 0.013 (mol C_2H_4) × s^{-1} × (mol Ir_4)$^{-1}$. In previous reports[10,16] of ethene hydrogenation catalyzed by Al_2O_3-supported tetrairidium clusters it was demonstrated that the tetrahedral cluster framework did not change during operation at 298 K and 1 bar, in the presence of a C_2H_4 partial pressure of 260 mbar and H_2 at partial pressures ranging from 170 to 380 mbar. Thus, we infer that under similar conditions (an equimolar feed stream at 294 K and 1 bar) the structural changes taking place in the nuclearity of our working zeolite-supported metal species clusters were also negligible—thus, we were able to determine the catalytic properties of the mononuclear iridium complexes and the iridium clusters independently.

Tuning of Structure of Predominant Catalytic Species during Ethene Hydrogenation. The results summarized in the preceding paragraphs show that the supported mononuclear iridium complexes and the supported clusters approximated well as Ir_4 have comparable catalytic activities for ethene hydrogenation at 294 K. However, the results stated above show that the supported species undergo changes in structure at readily measurable rates, depending on the reactive atmosphere, when the temperature is raised to 353 K—these data indicate that one should expect changes in the structure of the catalytically active species as a result of changes in the composition of the reactive atmosphere.

Thus, the data indicate the opportunity to tune the catalyst (specifically, the ratio of clusters to mononuclear complexes) by varying the ratio of ethene to H_2 in the atmosphere in contact with the catalyst. The following experiments were carried out to characterize this tuning:

First the clusters approximated as Ir_4 were formed from the mononuclear complexes by the treatment described above, and then the catalytic ethene hydrogenation reaction was started at 353 K with an ethene-rich feed ($C_2H_4/H_2 = 4$, molar), and then feed composition was switched from ethene-rich to equimolar $C_2H_4 + H_2$ and then to H_2-rich ($C_2H_4/H_2 = 0.3$, molar). The experiment was continued by cycling of the feed composition with the catalyst at 353 K. The reactor was an EXAFS cell and the structural changes in the catalyst were characterized by time-resolved spectroscopy, with individual spectra collected with a time-resolution of 2 min/scan (representing a near optimum in the trade-off between data quality and the time resolution). The X-ray beam passed through the bed of catalyst particles near the upstream end so that the part of the catalyst that was characterized structurally was the part in contact with a reactive atmosphere corresponding to the feed composition.

The results demonstrate a cycling of the structure of the iridium species, as follows:

Fragmentation of Iridium Clusters during Reaction in Ethene-Rich Stream. The spectra demonstrate the transformation of the supported iridium ethene complexes present initially into clusters during the treatment in flowing H_2 at 1 bar as the temperature was ramped to 353 K.[12] The Ir−Ir coordination number increased from 0 to 3, indicating that the clusters, on average, were Ir_4; the Ir−Ir bonding distance was 2.65 ± 0.02 Å.[9,10,12,17] When the feed was then switched to an ethene-rich stream ($C_2H_4/H_2 = 4$, molar), with the reactor still at 353 K, the product gas stream still contained the catalytic reaction product ethane, with a trace of butenes.[18] The EXAFS spectra (Figures 1 and 2; also see Supporting Information) show a decline of the Ir−Ir contribution and the concomitant growing-in of Ir−low-Z-scatterer contributions (Ir−O and Ir−C) during the flow of the ethene-rich stream, illustrated by the decrease in intensity of a contribution characterized by an Ir−backscatterer distance of approximately 2.5 Å (as shown in the Fourier-transformed EXAFS data, Figure 1, prior to phase- and amplitude-correction) and an increase in intensity of another contribution (shown at approximately 1.7 Å in Figure 1). Results obtained by analysis of the data (as described in the section EXAFS Data Analysis) indicate that the Ir−Ir coordination number decreased from approximately 3 to 0.4 in 25 min as the Ir−O and Ir−C coordination numbers simultaneously increased to 1.7 and 1.9, respectively (Figure 2), demonstrating that the clusters were undergoing fragmentation in the excess of ethene.

The Ir−Ir coordination number stabilized at nearly 0.4, indicating the presence of a mixture of mononuclear iridium complexes and unfragmented clusters. We estimate that approximately 13% of the Ir atoms were present in clusters and the remainder was in mononuclear species at this stage of the experiment.[19] The Ir−O coordination number of 1.7 in the stabilized catalyst is consistent with this inference, because a

(16) Previous reports[10] of Al_2O_3-supported tetrairidium cluster catalysts for this reaction indicate the almost the same activity for a feed composition similar to that used in our catalyst testing experiments (52 mbar C_2H_4 and 52 mbar H_2) at 288 K and a total pressure of 1 bar (the value determined by interpolation of the reported data[10] is 0.013 (mol C_2H_4) × s^{-1} × (mol Ir)$^{-1}$).

(17) Li, F.; Gates, B. C. *J. Phys. Chem. B* **2003**, *107*, 11589–11596.

(18) Detected by monitoring the effluent gas stream by mass spectrometry done in association with IR experiments.

(19) The fraction of the Ir atoms present in the clusters for any average Ir−Ir coordination number was calculated by equating the contributions of the Ir atoms present in the clusters corresponding to the average Ir−Ir coordination number (obtained by multiplying the concentration of the Ir atoms present in the clusters by 3) to the average Ir−Ir coordination number obtained in the EXAFS data analysis. If 100% of the Ir atoms were present in clusters, then the contribution of these atoms to the average Ir−Ir coordination number would be 3, and if 100% of the Ir atoms were present in mononuclear complexes then the average Ir−Ir coordination number would be 0.

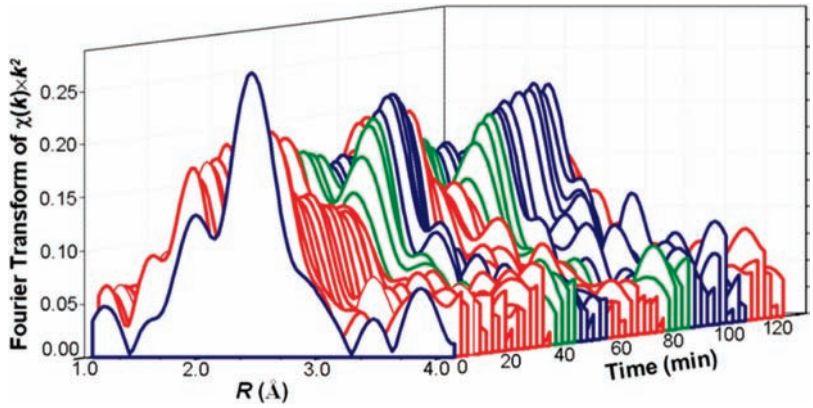

Figure 1. Radial distribution function determined from time-resolved EXAFS measurements of working catalyst formed from **1** and dealuminated zeolite Y recorded during changes in the C_2H_4/H_2 ratio: a mixture with $C_2H_4/H_2 = 4$ (molar, red), equimolar $C_2H_4 + H_2$ mixture (green), and $C_2H_4/H_2 = 0.3$ (molar, dark blue). Subsequent changes are indicated by the color coding. The peak at approximately 2.5 Å includes the Ir−Ir contribution, and that at approximately 1.7 Å includes the Ir−low-Z-scatterer contributions, Ir−O and Ir−C. The Δk and ΔR ranges were from at least 4.0 to 12.5 $Å^{-1}$ and from at least 1.2 to 3.2 Å, respectively.

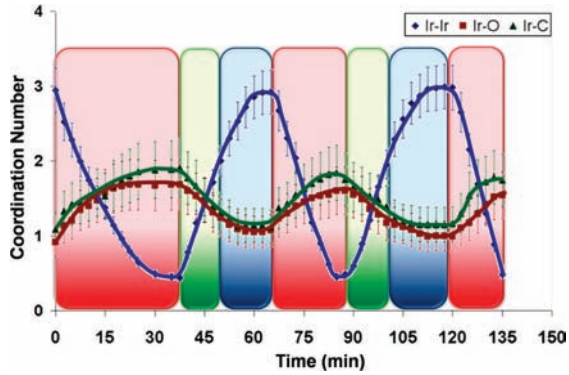

Figure 2. EXAFS analysis characterizing changes in the coordination numbers of the working catalyst formed from $Ir(C_2H_4)_2(acac)$ and dealuminated zeolite Y obtained by the fits with the recommended (three-shell) model. The data show the conversion of clusters approximated as Ir_4 to predominantly mononuclear iridium complexes, following a step-change in the feed to the flow reactor/EXAFS cell from H_2 to a mixture with $C_2H_4/H_2 = 4$ (molar, indicated with a red background). After 35 min, the feed composition was switched to equimolar $C_2H_4 + H_2$ (indicated with a green background). Later the feed ratio was switched to $C_2H_4/H_2 = 0.3$ (molar, indicated with a dark blue background). Subsequent changes are indicated by the color coding. The values of Δk and ΔR ranged from at least 4.0 to 12.5 $Å^{-1}$ and from at least 1.2 to 3.2 Å, respectively.

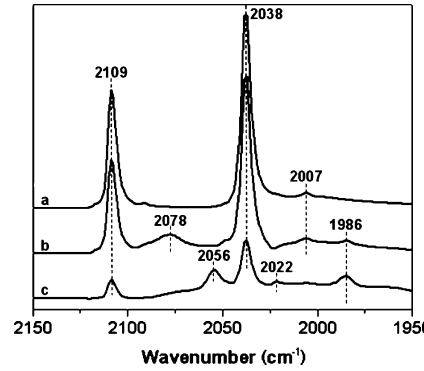

Figure 3. IR spectra characterizing: (a) $Ir(CO)_2$ on zeolite formed[17] by the reaction of $Ir(CO)_2(acac)$ precursor and dealuminated zeolite Y (the synthesis method was otherwise the same as that described for the synthesis of zeolite-supported $Ir(C_2H_4)_2$ complexes); (b) sample obtained from the reaction of dealuminated zeolite Y-supported $Ir(C_2H_4)_2$ complex with H_2 as the temperature was ramped to 353 K after the following set of treatments: flow of the ethene-rich mixture of ethene + H_2 for 25 min and then purging of the cell with helium, followed by injection of a pulse of 10 vol% CO in helium (5 mL); the spectrum was measured after the gas-phase CO had been purged from the flow system, as shown by mass spectrometric analysis of the product stream; (c) sample obtained from the reaction of a freshly prepared dealuminated zeolite Y-supported $Ir(C_2H_4)_2$ complex with H_2 as the temperature was ramped to 353 K after the following set of treatments: flow of the ethene-rich mixture of ethene + H_2 for 25 min and then flow of the H_2-rich feed for 25 min and then flow of helium to purge the cell, and then injection of a pulse of CO as described above in (b). All of these experiments were carried out at 353 K.

mononuclear complex requires 2 surface oxygen atoms to bond to the zeolite.[5]

Consistent with the EXAFS data, the XANES spectra at the Ir L_{III} edge (Supporting Information) (intensity at the edge position was normalized to 1 for each spectrum) show that intensity of the white line increased, consistent with oxidative fragmentation of some of the clusters in the ethene-rich stream. We emphasize that the change was slight; almost all of it took place within roughly the first 6 min of reaction, but the time is inexact because the change was so small; the XANES data do not provide much useful information.

The cluster break-up was not complete during the catalysis in the ethene-rich stream because the feed stream contained some H_2. When ethene alone was fed to the reactor (as stated above), the cluster break-up was complete, as shown by the disappearance of the Ir−Ir contribution in the EXAFS spectra.[12]

IR spectra confirm the formation of mononuclear iridium complexes from the clusters in the ethene-rich stream (Figure 3). The sample, after stabilization following the step-change in feed composition (Figures 1 and 2), was probed with a pulse of CO, and ν_{CO} bands indicative of Ir(I) gem-dicarbonyls were observed, at 2109 and 2038 cm^{-1}.[5] Because these ν_{CO} bands appeared essentially instantaneously after injection of the CO, we infer that mononuclear iridium complexes had been present before the injection, in agreement with the EXAFS data. Other (weak) ν_{CO} bands also appeared immediately after the injection, at 2078, 2007, and 1986 cm^{-1}, indicating the iridium clusters that were still present[15,17] and further confirming the EXAFS results.

Start of Reformation of Iridium Clusters during Reaction in Equimolar Ethene + H_2 Stream. Time-resolved EXAFS data show that the cluster break-up was reversed when the feed was switched from an ethene-rich mixture to equimolar ethene + H_2, indicated by an increase in the Ir−Ir coordination number accompanied by a decrease in the Ir−low-Z-scatterer contribu-

tions (Figures 1 and 2). Specifically, the data show the growing-in of the peak at 2.5 Å (Figure 1) indicating the Ir−Ir contribution and a decrease in intensity of the peak at 1.7 Å, indicating Ir−O and Ir−C contributions.

The Ir−Ir coordination number increased to approximately 1.7 as clusters formed in equimolar $C_2H_4 + H_2$, and the Ir−C and Ir−O coordination numbers each decreased to nearly 1.4 and 1.3, respectively (Figure 2). The data show that the mononuclear iridium complexes were converted only partially into clusters (we calculate that approximately 56% of the Ir atoms were present in clusters[19]).

Continuation of Reformation of Iridium Clusters during Reaction in H_2-Rich Stream. When the feed was changed to a H_2-rich mixture ($C_2H_4/H_2 = 0.3$), the Ir−Ir coordination number increased to approximately 3, indicating, on average, Ir_4 clusters. The Ir−C and Ir−O coordination numbers decreased correspondingly (Figure 2). The stabilized Ir−Ir distance (2.65 Å ± 0.02) is consistent with the bonding distance in typical Ir_4 clusters,[9,10,12,17] such as $Ir_4(CO)_{12}$ in NaY zeolite.[17] Still, the catalyst was active for ethene hydrogenation, with product stream containing ethane together with traces of butenes.[18]

When the feed composition changed to equimolar $C_2H_4 + H_2$, the white-line intensity of the XANES spectra decreased slightly, and then when the composition was changed to a H_2-rich mixture, it stayed almost constant. These results are again consistent with the EXAFS data but provide little useful information.

Further evidence on the reformation of clusters was obtained by using CO to probe the structures present in the catalyst. IR spectra recorded after injection of a CO pulse following the hydrogenation reaction under the conditions stated immediately above confirm these EXAFS results: intense bands appeared at 2108, 2056, 2038, and 1986 cm^{-1}, and a weak band appeared at 2022 cm^{-1}, consistent with tetrairidium carbonyl clusters (similar, but, because of the influence of the support and various ligands, not quite the same as those reported for NaY zeolite-supported $Ir_4(CO)_{12}$)[17] (Figure 3). This spectrum is contrasted with that of the sample exposed to the ethene-rich stream, which is characterized by much less intense bands representative of iridium clusters. Because the ν_{CO} bands formed essentially instantaneously after injection of the CO, we infer that the iridium clusters were present before the injection. The IR spectra (Figure 3) do not rule out mononuclear iridium complexes, because both tetrairidium carbonyl clusters and Ir(I) gem-dicarbonyls have IR bands at 2108 and at 2038 cm^{-1}; however, bands at 2056 and 1986 cm^{-1} confirm the presence of clusters.[17,20]

Reversibility of Dynamic Structural Changes of Active Species. As the experiment continued, the feed composition was switched repeatedly to cause the predominant form of the catalyst to switch repeatedly between Ir_4 clusters and mononuclear complexes (Figures 1 and 2). Thus, the data show how to reversibly tune the catalyst structure at the molecular scale by choice of the feed composition; the tuning leads to variations of the proportions of two forms of catalytically active species: mononuclear iridium complexes and iridium clusters that are well approximated as Ir_4.

Generalizing the Results. There are ample demonstrations of the role of reactants in converting surface structures into structures that are catalytically active and essentially molecular,[21,22] but tuning of such supported structures has heretofore been unreported, because the structures of these active species in a typical supported catalyst are extremely complicated, which makes it impossible to characterize the molecular-scale structural changes. Now, by using a zeolite-supported iridium catalyst involving essentially two types of structurally simple active species with interchangeable structures (mononuclear species and clusters), and by taking advantage of their high degree of uniformity—and of the tendency of the cluster formation to stop at extremely small clusters (approximately Ir_4), we have demonstrated how to control the active species by controlling the feed composition during ethene hydrogenation catalysis.

The results presented here must extend to other group-8 supported metal catalysts, as these metals are readily converted between mononuclear complexes and clusters, and both forms may be catalytically active.[11,23,24] We suggest that, although it might not usually be evident, active sites in solid catalysts, even beyond supported metals, commonly undergo structural changes resulting from changes in operating conditions.

However, such changes are usually neglected in the interpretation of reaction kinetics data—as the feed composition is varied to determine reaction rates for various reactant conditions. Thus, it was not feasible to determine fundamentally interpretable kinetics of ethene hydrogenation with our catalyst at temperatures high enough to facilitate changes in the catalyst structure on the time scale of kinetics measurements. Determinations of the rate of reaction as a function of reactant composition would fall short of providing insight into the reaction mechanism—as there would be more than one mechanism, corresponding to the different active sites.

Conclusions

We report real-time characterization of structural changes at the molecular level in a dealuminated zeolite Y-supported molecular iridium catalyst during ethene hydrogenation catalysis. Time-resolved EXAFS data demonstrate the reversible interconversion of mononuclear iridium complexes and tetrairidium clusters inside zeolite Y cages—thus changes in the concentration of the predominant catalytic species—resulting from changes in the C_2H_4/H_2 ratio at 353 K. Complementary IR experiments with CO as a probe molecule confirm the structural changes. These results are first to demonstrate such changes at the molecular level in a working supported catalyst.

Experimental and Data Analysis Section

Materials and Sample Preparation. Supported iridium complexes were prepared by the reaction of complex **1**[7] with highly dealuminated HY zeolite (Zeolyst International; Si/Al = 30 (atomic)), as before.[5] The catalyst Ir content was 1.0 wt %. H_2

(20) Under some conditions, CO oxidatively fragments iridium clusters, but the high intensities of the bands characteristic of our clusters indicate that little, if any, such fragmentation occurred after the CO injection; thus, we infer that the concentration of CO was low enough to minimize cluster break-up under the conditions of these experiments. The results consequently justify our approach in probing the nuclearity of the iridium species with IR spectroscopy and pulses of CO; see: Solymosi, F.; Novak, E.; Molnar, A. *J. Phys. Chem.* **1990**, *94*, 7250–7255.

(21) McCann, D. M.; Lesthaeghe, D.; Kletnieks, P. W.; Guenther, D. R.; Hayman, M. J.; Speybroeck, V. V.; Waroquier, M.; Haw, J. F. *Angew. Chem., Int. Ed.* **2008**, *47*, 5179–5182.
(22) Tada, M.; Akatsuka, Y.; Yang, Y.; Sasaki, T.; Kinoshita, M.; Motokura, K.; Iwasawa, Y. *Angew. Chem., Int. Ed.* **2008**, *47*, 9252–9255.
(23) Vajda, S.; Pellin, M. J.; Greeley, J. P.; Marshall, C. L.; Curtiss, L. A.; Ballentine, G. A.; Elam, J. W.; Catillon-Mucherie, S.; Redfern, P. C.; Mehmood, F.; Zapol, P. *Nat. Mater.* **2009**, *8*, 213–216.
(24) Mondloch, J. E.; Yan, X.; Finke, R. G. *J. Am. Chem. Soc.* **2009**, *131*, 6389–6396.

was supplied by Airgas (99.999%) or generated by electrolysis of water in a Balston generator (99.99%) and purified by passage through traps containing reduced Cu/Al_2O_3 and activated zeolite 4A to remove traces of O_2 and moisture, respectively. He (Airgas, 99.999%) and C_2H_4 (Airgas, 99.99%) were purified by passage through similar traps. CO (Matheson, 99.999%), in a 10% mixture in He, was purified by passage through a trap containing activated α-Al_2O_3 particles and zeolite 4A to remove any traces of metal carbonyls from high-pressure gas cylinders and moisture, respectively. Highly dealuminated HY zeolite (DAY zeolite) (Zeolyst International, CBV760), with a Si/Al atomic ratio of approximately 30, was calcined in O_2 at 773 K for 4 h and evacuated for 16 h at 773 K, isolated, and stored in an argon-filled glovebox (MBraun) until it was used. *n*-Pentane solvent (Fisher, HPLC grade) was dried and purified by column chromatography (Grubbs apparatus, MBraun SPS) in the presence of argon.

IR Spectroscopy. Transmission IR spectra of catalysts in a flow reactor/cell (In-situ Research Institute, South Bend, IN) were measured with a spectral resolution of 2 cm^{-1} as before;[5] each spectrum is the average of 128 scans. Each sample was pressed into a thin wafer and loaded into the cell (In-situ Research Institute, Inc., South Bend, IN) in the argon-filled glovebox. The cell allowed recording of spectra while gas (He, H_2, C_2H_4, and CO, alone or in combination) flowed around and through the wafer, sometimes as the temperature was ramped. In some experiments, pulses of CO in helium flowed through the cell; each pulse consisted of 5 mL of CO (10 vol% in helium) flowing at 100 mL/min.

Ethene Hydrogenation Catalysis in a Tubular Plug-Flow Reactor. Ethene hydrogenation catalysis was carried out in a conventional laboratory once-through tubular plug-flow reactor as the effluents produced by the reaction were monitored with a mass spectrometer. The catalyst (30 mg), diluted with particles of inert, nonporous α-Al_2O_3 in a mass ratio of Al_2O_3 to catalyst of 30:1, was loaded into the reactor in the argon-filled glovebox. The feed ethene and H_2 partial pressures were each 40 mbar. Details of the reaction experiments and product analysis by gas chromatography are as described elsewhere.[5] Conversions of ethene to ethane were < 5%, and the reactor is inferred to have operated in the differential mode, determining reaction rates directly. We report a comparison of the catalytic activities of mononuclear iridium complexes and Ir_4 clusters at 294 K and a single feed composition. Such data could not be obtained at temperatures substantially higher than this, because the catalyst structure too rapidly changed as a function of the reactant composition, and it was not feasible to compare the activities of the two different forms of the catalyst under the same conditions, as demonstrated above.

X-Ray Absorption Spectroscopy. Time-resolved X-ray absorption spectra were recorded at X-ray beamline MR-CAT at the Advanced Photon Source at Argonne National Laboratory. The storage ring electron energy and ring currents were 7.0 GeV and 105 mA, respectively. Data were recorded for 2 min to determine each spectrum in transmission mode. Powder samples were loaded into an EXAFS cell/reactor[25] inside an argon-filled glovebox at the synchrotron.

During the initial treatment of the catalyst in flowing H_2, the temperature was increased to 353 K and then kept constant. Flow of reactant gas started at this temperature, and the feed composition was subsequently varied as stated in the captions of Figures 1 and 2. Total flow rate was 50 mL (NTP)/min. During these treatments, to make the spectroscopic data for all the samples comparable and dependent on the composition of the feed to the cell, the beam was focused near the inlet, and the beam diameter was kept small (approximately 2 mm).

EXAFS Data Analysis. Analysis of the EXAFS data was carried out with the software ATHENA of the IFEFFIT[26] package and the software XDAP,[27] details are given elsewhere[5,12] and in the Supporting Information. Structural models postulated for the supported iridium species were compared with the EXAFS data. The models were chosen to include all plausible absorber−backscatterer combinations suggested by the synthesis chemistry and IR spectra of our samples, as well as the chemistry of related samples.[5,12] Various models with various numbers of shells were considered in the data fitting.

Reference files used in the fitting, with backscattering amplitudes and phase shifts for Ir−Ir, Ir−O, Ir−C, and Ir−Al contributions[28] were calculated with the software FEFF7.0[29] from crystallographic coordinates of the unit cells of the reference compounds iridium metal, $Ir(C_2H_4)_2(acac)$,[7] IrO_2, and Ir−Al alloy. Data analysis was carried out with unfiltered data by a "difference-file" technique;[30] iterative fitting was performed until optimum agreement was attained between the calculated k^1-, k^2-, and k^3-weighted EXAFS data (k is the wavenumber) and each postulated model.

The fitting was done in *R*-space with the Fourier-transformed chi data, and the quality of the fit was also checked in *k*-space (chi is the EXAFS function; *R* is the distance from the absorbing atom). The *k*- and *R*-ranges used in the fitting for each model are stated in the appropriate Figure captions and in a summary table in Supporting Information; the *k*-ranges were determined conventionally,[30] at the low end by where the background could be reliably separated from the total absorption and at the high end by where the signal became difficult to distinguish from the noise.[30] The *R*-ranges were determined as recommended[31] in the "difference file" method by considering each shell individually and including the full range over which a satisfactory fit could be obtained for each individual shell.

The number of parameters used in the fitting with the recommended model was less than the statistically justified number computed with the Nyquist theorem:[31] $n = (2\Delta k \Delta R/\pi) + 2$, where Δk and ΔR are the *k*- and *R*-ranges used in the fitting, respectively. Specifically, for this three-shell fit,[28] the values of Δk and ΔR ranged from at least 4 to 12.5 $Å^{-1}$ and from at least 1.2 to 3.2 Å, respectively, implying that the number of justified parameters in the worst case was at least 13 (12 were used in the fit); however, the typical number of justified parameters was about 16 (Tables SI-1 to SI-3 in the Supporting Information include the value for each of the data sets).

For efficiency in the data reduction, the most thorough EXAFS analyses were done for key samples to provide starting points; then quicker, less thorough analyses were done by interpolation for the samples with intermediate structures (more precisely, mixtures of structures) that formed during the transformations. This procedure is justified because the changes undergone by the samples during the treatments were gradual, as was demonstrated by the results of the analyses.

The data obtained when the temperature of the sample reached to 353 K for the first time in H_2 flow were chosen as the starting point for the data analysis because the ethene hydrogenation reaction was started after this point; thus, this data set is considered as key for the data analysis. Therefore, the most thorough analysis was performed with this data set (and with some others, as stated elsewhere in this document). The fit quality is illustrated for a typical

(25) Odzak, J. F.; Argo, A. M.; Lai, F. S.; Gates, B. C.; Pandya, K.; Feraria, L. *Rev. Sci. Instrum.* **2001**, *72*, 3943–3945.
(26) Newville, M. *J. Synchrotron Rad.* **2001**, *8*, 322–324.
(27) Vaarkamp, M.; Linders, J. C.; Koningsberger, D. C. *Physica B* **1995**, *209*, 159–160.
(28) Alternatively, a four-shell model was also applied, as described in detail in the EXAFS Data Analysis Section and in the Supporting Information.
(29) Zabinsky, S. I.; Rehr, J. J.; Ankudinov, A.; Albers, R. C.; Eller, M. J. *Phys. Rev. B.* **1995**, *52*, 2995–3009.
(30) (a) Kirlin, P. S.; van Zon, F. B. M.; Koningsberger, D. C.; Gates, B. C. *J. Phys. Chem.* **1990**, *94*, 8439–8450. (b) van Zon, F. B.; Koningsberger, D. C.; van't Blik, H. F. J.; Sayers, D. E. *J. Chem. Phys.* **1985**, *82*, 5742–5754. (c) Guzman, J.; Gates, B. C. *J. Catal.* **2004**, *226*, 111–119. (d) Koningsberger, D. C.; Mojet, B. L.; van Dorssen, G. E.; Ramaker, D. E. *Top. Catal.* **2000**, *10*, 143–155.
(31) Stern, E. A. *Phys. Rev. B* **1991**, *43*, 8850–8860.

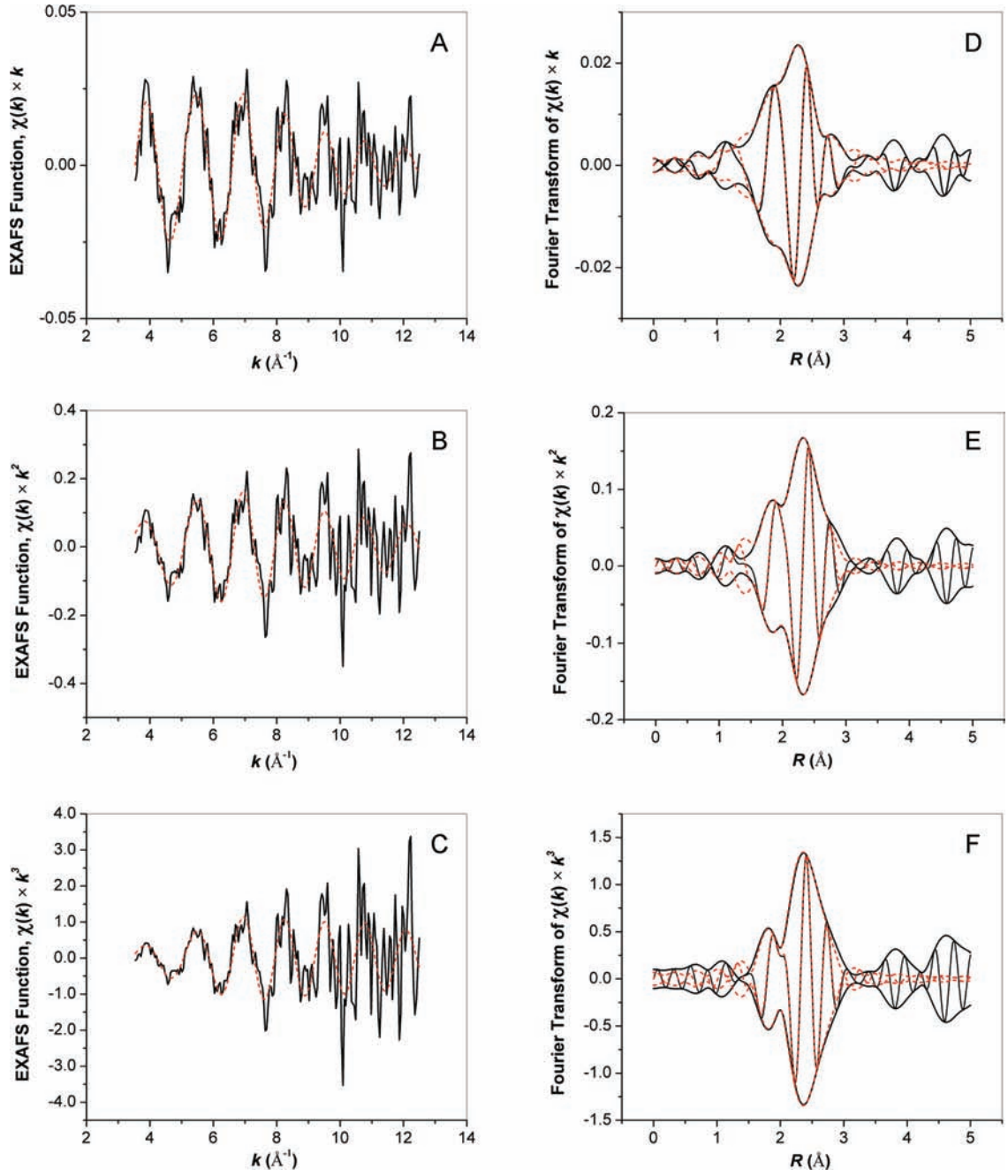

Figure 4. Results showing the goodness of fits from the EXAFS data analysis for the sample formed from the reaction of **1** with DAY zeolite that had been calcined at 773 K. The sample in flowing H_2 was heated to 353 K before the data were collected as H_2 flow continued at this temperature. EXAFS function, χ (solid line), and calculated contribution (dotted line); A, k^1-weighted; B, k^2-weighted; C, k^3-weighted; Imaginary part and magnitude of the Fourier transform of data (solid lines) and calculated contributions (dotted lines); D, k^1-weighted; E, k^2-weighted; F, k^3-weighted ($\Delta k = 3.5-12.6$ Å^{-1}).

data set in Figure 4 (further details are given in Supporting Information, where goodness of fit information is given for all the data, and below).

The analysis resulted in two plausible fit models, a three-shell model and a four-shell model. The model selection was made on the basis of standards recommended by the International EXAFS Society Standards and Criteria Committee. The three-shell model includes the plausible contributions Ir−Ir, Ir−O, and Ir−C, and the four-shell model includes Ir−Ir, Ir−O, Ir−C, and Ir−Al.

The following section includes the statistical justification and physical comparison of these two models for the example data set characterizing the initial condition of the sample used for the experiment (obtained when the temperature reached to 353 K in H_2 flow for the first time).

Statistical Justification of Model I and Model II. Model I. The three-shell fit model includes the following shells: Ir−Ir, Ir−O, and Ir−C. All of these contributions were fitted by using the best combination of reference files representing the bonding, as summarized above.

The results characterizing the fit parameters obtained with Model I for each of the data sets are summarized in Table SI-1. For example, Figures SI-1 to SI-4 in the Supporting Information show the results of the EXAFS data analysis for the initial data set, which was chosen on the basis stated above. The *k*-range for the fit is from 3.5 to 12.6 Å^{-1} and the *R*-range is from 1.2 to 3.5 Å (Supporting Information, Table SI-3 and Figures SI-1 to SI-4). The Nyquist theorem[31] indicates that the number of statistically justified

fit parameters is 16, which exceeds the number used in fitting (12) with this model.

As shown in the Supporting Information, Figures SI-1 to SI-4, the overall fit of the data on the basis of fits of individual contributions is satisfactory. The goodness of fit value for this example data set was calculated to be 2.3 by the following formula:

$$\text{goodness of fit} = \frac{\nu}{\text{NPTS}(\nu - N_{\text{free}})} \sum_{i=1}^{\text{NPTS}} \left(\frac{\chi_{\text{exp},i} - \chi_{\text{model},i}}{\sigma_{\text{exp},i}} \right)^2 \quad (1)$$

where χ_{model} and χ_{exp} are the fit and experimental EXAFS respectively, σ_{exp} is the error in the experimental results, ν is the number of independent data points in the fit range, and NPTS is the actual number of data points in the fit range.

The *k*-range and *R*-range values for the fits obtained for all of the data points during the experiment, as well as the goodness of fit parameters, are given in the Supporting Information, Table SI-3. This table shows that the number of justified parameters ranges from 13 to 17—thus was always more than 12, and the goodness of fit parameters range from 1.9 to 3.5 with this three-shell fit model.

Model II. The four-shell model includes the following shells: Ir−Ir, Ir−O, Ir−C, and Ir−Al. All of these contributions were fitted by using the best combination of reference files representing the bonding, as summarized above. The Ir−Al contribution (this is the additional shell in the four-shell model) is characterized by a coordination number ranging from 0.4 (with an estimated error of approximately ± 0.1) for samples containing iridium predominantly in clusters to 0.8 (with an estimated error of approximately ± 0.2) for samples containing iridium predominantly in mononuclear complexes. These values make good physical sense: the latter indicates, within error, the presence of one cationic iridium complex per aluminum site, as expected, and the former is consistent with the location of the clusters at these sites.

The results characterizing the fit parameters obtained with Model II for each of the data sets are summarized in the Supporting Information, Table SI-2. Figures SI-5 to SI-9 in the Supporting Information show the results of the analysis for the same example data set chosen for Model I. The *k*-range for the fit is from 3.5 to 12.6 $Å^{-1}$ (Supporting Information, Table SI-3 and Figures SI-5 to SI-9). Figure SI-8 in the Supporting Information indicates that the fit for the Ir−C shell represents the data satisfactorily for an *R*-range of from 1 to 2.7 Å, and similarly Figure SI-6 in the Supporting Information indicates that the fit for the Ir−Ir shell is valid for an *R*-range from 1.4 to 3.5 Å. Thus, the overall significant ΔR was determined to extend from 1 to 3.5 Å (which represents the full range for the combination of these two cases).[31] Thus, for these *k*- and *R*-ranges the Nyquist theorem[31] indicates that the number of statistically justified fit parameters is 17, which exceeds the number used in fitting (16) with this model. The ΔR value was determined as described above.[31]

Again, as in the case of the Model I, the overall fit of the data on the basis of fits of individual contributions is satisfactory for this model (Supporting Information, Figures SI-5 to SI-9). The goodness of fit was calculated as 8.9 by the equation given above for this example data set. The *k*-range and *R*-range values for the fits obtained for all of the data points and the goodness of fit parameters are summarized in the Supporting Information, Table SI-3. This table shows that the number of justified parameters ranges from 17 to 19—thus always more than 16, and the goodness of fit parameter values range from 2.1 to 9.3 with this four-shell fit model.

Comparison of Model I and Model II: The goodness of fit parameters for each of the data sets summarized in the Supporting Information, Table SI-3 and Figures SI-1 to SI-9, indicate the typical fit quality given for a representative data set.

Model I is preferred because it is a more conservative choice than Model II, involving three and not four shells and providing statistically a better fit than Model II as indicated by the goodness of fit values, as summarized in the Supporting Information, Table SI-3. Therefore, in Figures 2 and 4, results obtained with this model are presented, and the presentation of results above is based on this model.

Nonetheless, we judge that Model II has sufficient merit to warrant presentation, and we report the results obtained with this model in Figure SI-11.

We emphasize that changes in the Ir−Ir contribution obtained with the two models over the course of the experiment, both in terms of distance and coordination number, are the same within the estimated error (Supporting Information, Tables SI-1 and SI-2). This comparison demonstrates that the central conclusions of this work regarding cluster break-up and formation do not depend on which of the two models was used to fit the EXAFS data, bolstering the validity of our main conclusions derived from the changes in the metal−metal coordination numbers (formation and break-up of the metal clusters) with the changes in the feed composition.

Acknowledgment. This research was supported by the U.S. Department of Energy, Office of Energy Research, Basic Energy Sciences, grant FG02-04ER15600. We acknowledge beam time and support of the DOE Division of Materials Sciences for its role in the operation and development of beamline MR-CAT at the Advanced Photon Source at Argonne National Laboratory. We thank the beamline staff for assistance.

Supporting Information Available: Tables summarizing EXAFS fit and goodness of fit parameters of the individual shells for each of the EXAFS data sets (for both Models I and II), the values of Δk and ΔR ranges used in the EXAFS data fitting (for both Model I and II), plots showing fit qualities of each individual shells used in the EXAFS data fitting (for both Models I and II), plot showing the variation of coordination numbers obtained with Model II, XANES spectra recorded simultaneously with the time-resolved EXAFS spectra, and plots showing break-in of the catalyst (both for supported mononuclear complexes and tetrairidium clusters) during operation in a once-through flow reactor, IR spectra of the silanol groups showing the reverse spillover process. This material is available free of charge via the Internet at http://pubs.acs.org.

JA906553N